Anchors no more: using peculiar velocities to constrain H_0 and the primordial Universe without calibrators

Piras, Davide; Sorrenti, Francesco; Durrer, Ruth; Kunz, Martin

How to cite

PIRAS, Davide et al. Anchors no more: using peculiar velocities to constrain H_0 and the primordial Universe without calibrators. In: Journal of cosmology and astroparticle physics, 2025, vol. 2025, n° 09, p. 005. doi: 10.1088/1475-7516/2025/09/005

This publication URL: https://archive-ouverte.unige.ch/unige:188704
Publication DOI: 10.1088/1475-7516/2025/09/005

Journal of Cosmology and Astroparticle Physics
An IOP and SISSA journal

Received: *May 9, 2025*
Accepted: *July 31, 2025*
Published: *September 1, 2025*

Anchors no more: using peculiar velocities to constrain H_0 and the primordial Universe without calibrators

Davide Piras[a,b,1] **Francesco Sorrenti**[b,1] **Ruth Durrer**[b] **and Martin Kunz**[b]

[a] *Centre Universitaire d'Informatique, Université de Genève, 7 route de Drize, 1227 Genève, Switzerland*
[b] *Département de Physique Théorique, Université de Genève, 24 quai Ernest Ansermet, 1211 Genève 4, Switzerland*

E-mail: davide.piras@unige.ch, francesco.sorrenti@unige.ch, ruth.durrer@unige.ch, martin.kunz@unige.ch

Abstract: We develop a novel approach to constrain the Hubble parameter H_0 and the primordial power spectrum amplitude A_s using type Ia supernovae (SNIa) data. By considering SNIa as tracers of the peculiar velocity field, we can model their distance and their covariance as a function of cosmological parameters without the need of calibrators like Cepheids; this yields a new independent probe of the large-scale structure based on SNIa data without distance anchors. Crucially, we implement a differentiable pipeline in `JAX`, including efficient emulators and affine sampling, reducing inference time from years to hours on a single GPU. We first validate our method on mock datasets, demonstrating that we can constrain H_0 and $\log 10^{10} A_s$ within 10% and 15%, respectively, using $\mathcal{O}(10^3)$ SNIa. We then test our pipeline with SNIa from an N-body simulation, obtaining 6%-level unbiased constraints on H_0 with a moderate noise level. We finally apply our method to Pantheon+ data, constraining H_0 at the 15% level without Cepheids when fixing A_s to its *Planck* value. On the other hand, we obtain 20%-level constraints on $\log 10^{10} A_s$ in agreement with *Planck* when including Cepheids in the analysis. In light of upcoming observations of low redshift SNIa from the Zwicky Transient Facility and the Vera Rubin Legacy Survey of Space and Time, surveys for which our method will develop its full potential, we make our `veloce` (https://github.com/dpiras/veloce) code publicly available.

Keywords: cosmological parameters from LSS, supernova type Ia - standard candles, Machine learning, cosmological simulations

ArXiv ePrint: 2504.10453

[1] Equal contribution.

https://doi.org/10.1088/1475-7516/2025/09/005

JCAP09(2025)005

Contents

JCAP09(2025)005

1 Introduction

Type Ia supernovae (SNIa) are the best standard candles in cosmology up to date. They have been instrumental in detecting the accelerated expansion of the Universe [1, 2] and supporting the dark energy hypothesis [3]. Within the standard flat ΛCDM cosmology, the recent expansion history is determined by the matter density $\Omega_{\rm m}$ and Hubble constant H_0, which can be both inferred from the luminosity distance-redshift relation $d_{\rm L}(z)$ in a Friedmann-Lemaître (FL) universe. For this reason, SNIa are important for joint measurements of H_0 and $\Omega_{\rm m}$, see e.g. ref. [4].

However, SNIa are not perfect standard candles, and they need to be normalized with the help of distance anchors; in particular, the Hubble constant is perfectly degenerate with the absolute distance normalization. Moreover, the Universe is not a perfect FL universe, but its matter distribution and geometry are perturbed, while the redshifts of SNIa are affected by the peculiar velocities of their host galaxies. So far, these velocities have mostly been modeled using the velocity field reconstruction approach to convert the CMB-corrected redshifts into so-called 'Hubble diagram redshifts', $z_{\rm HD}$ [5], or through a Bayesian hierarchical model marginalizing over unknown cosmological redshifts and peculiar velocities [6].

In this work, we consider a different approach to treat velocities, based on ref. [7]. We correct the SNIa redshifts for peculiar velocities by adding them to the velocity power spectrum covariance. Like the matter power spectrum, this covariance also depends on the cosmological parameters H_0 and Ω_m, in addition to the initial power spectrum described by the amplitude A_s and the spectral slope n_s. The variance of the SNIa data therefore also contains information about H_0 which is completely independent of any distance anchor like the Cepheids. This is particularly interesting in light of the so-called Hubble tension [8–10] as it provides an additional independent way to measure the low-redshift Hubble constant from supernova data.

Other works have looked into constraining the growth of structure from the power spectrum of peculiar velocities, using both simulated and real data. For instance, in ref. [11] the authors used both simulated data and various real datasets like the COMPOSITE catalogue [12] to estimate the matter power spectrum, finding good agreement with ΛCDM, while ref. [13] constrained the growth rate of structures using the 6dF Galaxy Survey [14]. Similar analyses were performed in ref. [15] using the 2MASS Tully-Fisher survey [16], and in ref. [17] using the Supercal dataset [18], respectively. In ref. [19] a forecast of the constraints of the growth rate for ZTF (Zwicky Transient Facility, [20]) was performed using an earlier version of the `FLIP` package [21], while in ref. [22] the impact of peculiar velocities on the measure of H_0 for the ZTF second data release [23] was estimated. Additionally, ref. [24] estimated the H_0 uncertainty due to peculiar velocities in the Hubble flow. The velocity power spectrum also proved to be useful in testing the standard cosmological model assuming distinct estimates of the matter density, as done in ref. [25].

In our work, we specifically focus on H_0 and A_s, with a detailed treatment of the velocity covariance. We develop an efficient and differentiable pipeline that combines neural network emulators and affine sampling, and we validate it on mock data and N-body simulations. We finally apply our pipeline to Pantheon+ data [26], showing that in principle supernova surveys can constrain the Hubble parameter without the need for distance anchors. While results from present data are not yet conclusive, we envision that our method will fully unlock its potential with upcoming data like ZTF which include thousands of low-redshift SNIa [23].

This paper is structured as follows. In section 2 we describe our theoretical model, while in section 3 we present the implementation pipeline. We then validate our approach on a mock dataset, before applying it to an N-body simulation as well as to the Pantheon+ data, in section 4. We conclude in section 5.

2 Theoretical model

We model the SNIa magnitude data with a Gaussian likelihood, which is given by:

$$\log(\mathcal{L}) = -\frac{1}{2}\Big[\Delta\mu_n\, C^{-1}_{mn}\, \Delta\mu_m + \log(\det C_{mn}) + k\log(2\pi)\Big], \tag{2.1}$$

where a summation over the repeated indices m and n is implied, and k is the dimension of the covariance C, namely the number of SNIa in our dataset. The vector $\Delta\mu_i$ is given by:

$$\Delta\mu_n = \begin{cases} \mu_n - \mu_{\mathrm{ceph},n} + \delta\mathrm{M} & \text{if } n\text{-th SNIa galaxy hosts Cepheids,} \\ \mu_n - \mu_\mathrm{model}(z^\mathrm{hel}_n) + \delta\mathrm{M} & \text{otherwise.} \end{cases} \tag{2.2}$$

JCAP09(2025)005

Here, μ_n is the observed magnitude of the n-th SNIa, and δM is a normalization parameter, i.e. the magnitude shift. SNIa in galaxies that also host Cepheids (providing a measurement of their normalized magnitude $\mu_{\rm ceph}$) are uniquely used to determine δM which would otherwise be perfectly degenerate with H_0. The theoretical distance modulus $\mu_{\rm model}$ is related to the luminosity distance via:[1]

$$\mu_{\rm model} = 5\log_{10}\left(\frac{\langle d_{\rm L}(z^{\rm hel},\mathbf{n})\rangle}{\rm Mpc}\right) + 25\,, \tag{2.3}$$

where

$$d_{\rm L}(z,\mathbf{n}) = \bar{d}_{\rm L}(z)\Bigg[1 + \frac{1}{\mathcal{H}(z)r(z)}\mathbf{n}\cdot(\mathbf{v}_\odot - \mathbf{v}(z,\mathbf{n})) - \frac{\mathbf{n}\cdot\mathbf{v}(z,\mathbf{n})}{c} - \\ \Phi - \left(1-\frac{1}{\mathcal{H}r}\right)\left(\Psi + \int_0^r dr'(\dot{\Psi}+\dot{\Phi})\right) + \int_0^r \frac{dr'}{r}\left(1 - \frac{(r-r')}{2r'}\Delta_\Omega\right)(\Psi+\Phi)\Bigg]. \tag{2.4}$$

This is the observable luminosity distance to the measured redshift z at first order in perturbation theory. Here, $\mathbf{v}_\odot$ is the peculiar velocity of the solar system (measured by the CMB dipole), $\mathbf{n}$ is the direction of the SNIa, and $\mathbf{v}(z,\mathbf{n})$ its peculiar velocity. Furthermore, $\mathcal{H} = \mathcal{H}(z) = \dot{a}/a^2 = H/a$ is the comoving Hubble parameter, $H = H(z)$ is the physical Hubble parameter, a is the scale factor, and $\bar{d}_{\rm L}$ is the unperturbed luminosity distance defined in eq. (2.7) below. Furthermore, $r = r(z)$ is the comoving distance out to redshift z such that $\bar{d}_L(z) = r(z)(1+z)$, and the variables Φ and Ψ are the so-called gauge invariant Bardeen potentials that describe scalar perturbations of the metric; in a ΛCDM cosmology, and at the times and scales relevant here, they are the same and equal to the Newtonian gravitational potential. Δ_Ω denotes the 2D Laplacian on the sphere of directions $\mathbf{n}$. In this full formula the second line has to be evaluated at the position of the supernova given by z and $\mathbf{n}$ at first order in perturbation theory [27]. In the present work, we only take into account the contributions from velocities given in the first line, which largely dominate at low redshift, $z \ll 1$. At high redshifts ($z \gtrsim 0.5$) the lensing contribution given by the last integrated term is the most relevant: as it is usually done, we model it as an error proportional to z^2. The other relativistic contributions from the gravitational potential are the integrated Sachs-Wolfe term, Shapiro time delay, and the gravitational potential at the source. However, they (and some additional terms at the position of the observer which we have not written as they only contribute a constant) remain always very subdominant, see e.g. refs. [27, 28] for a numerical evaluation.

The terms we shall consider in this work are the Doppler terms given in the first line of eq. (2.4). We express them in terms of their measured, heliocentric redshift $z^{\rm hel}$ as:

$$d_{\rm L}(z^{\rm hel},\mathbf{n}) \simeq \bar{d}_{\rm L}(z^{\rm hel})\left[1 + \frac{1}{H(z^{\rm hel})\bar{d}_{\rm L}(z^{\rm hel})}\mathbf{n}\cdot(\mathbf{v}_\odot - \mathbf{v}(z^{\rm hel},\mathbf{n})) - \frac{\mathbf{n}\cdot\mathbf{v}(z^{\rm hel},\mathbf{n})}{c}\right]. \tag{2.5}$$

This perturbed luminosity distance now depends on direction and can be expanded in spherical harmonics. We shall model it by a monopole, a dipole that models the bulk velocity field, and a quadrupole that models large scale variations of the velocity field. We shall take variations of the velocity field on smaller scales into account in the covariance as a correlated error determined by the velocity power spectrum.

[1] We always indicate the base of the logarithm unless it is the natural one.

JCAP09(2025)005

When taking the ensemble average of eq. (2.5) in terms of the CMB-corrected redshift $z = z^{\rm hel} - (1+z)\mathbf{v}_\odot \cdot \mathbf{n}/c$ (i.e. correcting $z^{\rm hel}$ for the observer motion, with c ths speed of light), we find:

$$\langle d_{\rm L}(z,\mathbf{n})\rangle = \bar{d}_{\rm L}(z)\,. \tag{2.6}$$

$\bar{d}_{\rm L}(z)$ is the background luminosity distance, which in a flat ΛCDM model at late times is given by:

$$\bar{d}_{\rm L}(z) = c(1+z)\int_0^z \frac{dz'}{H(z')} = \frac{c(1+z)}{H_0}\int_0^z \frac{dz'}{\sqrt{\Omega_{\rm m}(1+z')^3+1-\Omega_{\rm m}}} = (1+z)r(z)\,. \tag{2.7}$$

Even though the ensemble average of $d_L(z)$ is $\bar{d}_L(z)$, the measured $d_{\rm L}(z)$ does not simply average to $\bar{d}_{\rm L}(z)$. This is a manifestation of cosmic variance: what we observe can easily be 1-2σ away from the ensemble average and we have no means to include its error other than by modeling it. Whether one has to do this up to multipole 2 or 10 depends on the quality of the data and on the angular coverage of the survey: if instrumental errors are small, more multipoles have to be modeled, while when the angular coverage is narrow, fewer multipoles can be modeled. In the present work we model the monopole, dipole and quadrupole of the Pantheon+ data, which have already been determined and discussed in a previous paper [29]. These additional contributions are not unexpected and are in good agreement with ΛCDM, as we have shown in ref. [29]; they would average out in a true ensemble average over many universes, but they do not average out in the data from one universe. Therefore, in our estimator for $\bar{d}_{\rm L}(z)$ in the case of real supernova data we subtract the maximum-a-posteriori monopole, dipole and quadrupole terms using the `scoutpip` package.[2]

We write the total covariance matrix C as a sum of an error term, $C^{(\rm e)}_{mn}$ coming from measurement errors in the SNIa magnitudes including a lensing contribution $\propto z^2$, and a velocity-induced term, $C^{(\rm v)}_{mn}$, that describes the redshift fluctuations due to peculiar velocities:[3]

$$C_{mn} = C^{(\rm e)}_{mn} + C^{(\rm v)}_{mn}\,. \tag{2.8}$$

The error covariance matrix $C^{(\rm e)}$ is the error covariance of the SNIa data from which the peculiar velocity contribution is subtracted, while the velocity-induced covariance matrix $C^{(\rm v)}$ is due to the difference between the measured redshift z_n and the redshift of the background cosmology $\bar{z}_n$ induced by peculiar velocities. This leads to a difference $\delta z_n = (1+z_n)\frac{v_n}{c}$ between the measured and the cosmological redshift, where $v_n = \mathbf{n}_n \cdot \mathbf{v}_n$ is the peculiar velocity of the n-th object. Here we include this redshift change as an additional fluctuation $\delta\mu^{(v)}_n$ of the distance modulus [19] given by:

$$\frac{\log 10}{5}\delta\mu^{(\rm v)}_n = \left[\frac{c(1+z_n)^2}{d_{\rm L}(z_n)\,H(z_n)} - 1\right]\frac{v_n}{c}\,. \tag{2.9}$$

In appendix A we derive and discuss in detail this result, which is in agreement with ref. [19],

[2] https://github.com/fsorrenti/scoutpip.

[3] For the SNIa in Cepheid-hosting galaxies, the velocity-induced fluctuations affect both SNIa and Cepheids equally, so that this contribution to the covariance is not present for those entries. Moreover, we assume the intrinsic SNIa magnitude dispersion is fixed in $C^{(\rm e)}$, but we find consistent results when allowing it to vary.

JCAP09(2025)005

To obtain the velocity-induced covariance for the magnitudes, we start by considering the covariance of the radial component of the peculiar velocities. In our treatment, we neglect vorticity and first consider the linear velocity power spectrum from scalar perturbations, $P_{\rm v}$. The covariance matrix of peculiar radial velocities is then of the form:

$$C_{mn}^{(\rm v),\rm v} = \int \frac{4\pi k^2 \mathrm{d}k}{(2\pi)^3} W_{mn}(k) \left\langle v_m v_n \right\rangle = \int \frac{4\pi k^2 \mathrm{d}k}{(2\pi)^3} W_{mn}(k)\, P_{\rm v}\left(k, z_m, z_n\right), \tag{2.10}$$

where $P_{\rm v}\left(k, z_m, z_n\right)$ is the unequal-redshift velocity power spectrum and W_{mn} is a window function determined by the real space positions of the supernovae. To obtain the velocity-induced covariance matrix for the distance modulus μ_i, we multiply eq. (2.10) with the conversion factor B_{mn} obtained from eq. (2.9):

$$B_{mn} = \left(\frac{5}{c\,\log(10)}\right)^2 \left[\frac{c(1+z_m)^2}{d_{\rm L}(z_m)\,H(z_m)} - 1\right]\left[\frac{c(1+z_n)^2}{d_{\rm L}(z_n)\,H(z_n)} - 1\right]. \tag{2.11}$$

Note that B_{mn} is independent of H_0 as it cancels in the combination $d_{\rm L}(z)H(z)$. The covariance of the SNIa magnitudes from peculiar velocities is then:

$$C_{mn}^{(\rm v)} = B_{mn} \int \frac{4\pi k^2 \mathrm{d}k}{(2\pi)^3} W_{mn}(k)\, P_{\rm v}\left(k, z_m, z_n\right) \tag{2.12}$$

where the window function W_{mn} in eq. (2.12) is given by:

$$W_{mn}(k) = \sum_{i,j=1}^{3} n_{m,i}\, n_{n,j} \int \frac{\mathrm{d}^2\hat{k}}{4\pi} \hat{k}_i\, \hat{k}_j e^{ik\hat{\mathbf{k}}\cdot(\mathbf{r}_m - \mathbf{r}_n)}, \tag{2.13}$$

with $\mathbf{n}_m = \mathbf{r}_m/r_m$ and $\mathbf{n}_n = \mathbf{r}_n/r_n$ the directions of the m-th and n-th SNIa respectively, and i, j the spatial indexes. In appendix B we derive an analytic expression for this window function:

$$W_{mn}(k) = \frac{1}{3}\cos\alpha_{mn}\left[j_0(kR_{mn}) - 2j_2(kR_{mn})\right] + \frac{r_m r_n}{R_{mn}^2} j_2(kR_{mn})\sin^2\alpha_{mn}, \tag{2.14}$$

where α_{mn} is the angle between $\mathbf{r}_m$ and $\mathbf{r}_n$, j_ℓ is ℓ-th order spherical Bessel function and $R_{mn} = |\mathbf{r}_m - \mathbf{r}_n|$. For $m = n$ we have $W_{mm} = 1/3$. These results agree with the more involved derivation given in ref. [30].

2.1 The velocity power spectrum

Considering only linear perturbations, the velocity power spectrum $P_{\rm v}$ is given by:

$$\begin{aligned} P_{\rm v}(k, z_m, z_n) =& \left[\frac{\dot{D}_1(z_m)}{D_1(z_m)(1+z_m)}\right]\left[\frac{\dot{D}_1(z_n)}{D_1(z_n)(1+z_n)}\right]\frac{P_\delta(k, z_m, z_n)}{k^2} \\ =& \left[\frac{H(z_m)f(z_m)}{(1+z_m)}\right]\left[\frac{H(z_n)f(z_n)}{(1+z_n)}\right]\frac{P_\delta(k, z_m, z_n)}{k^2}, \end{aligned} \tag{2.15}$$

where $P_\delta(k)$ is the linear matter power spectrum, D_1 the linear growth function and f the growth rate. In a flat ΛCDM cosmology, which we assume in this work, D_1 is given by [31]:

$$D_1(z) = \frac{D_0}{(1+z)}\left[{}_2F_1\left(\frac{1}{3}, 1; \frac{11}{6}; 1 - \frac{1}{\Omega_{\rm m}(z)}\right)\right], \tag{2.16}$$

JCAP09(2025)005

where ${}_2F_1(a,b;c;d)$ is the confluent hypergeometric function [32] and D_0 is a normalization constant. The matter density parameter is

$$\Omega_{\rm m}(z) = \frac{\Omega_{\rm m}\,(1+z)^3}{\Omega_{\rm m}\,(1+z)^3 + (1-\Omega_{\rm m})}\,. \tag{2.17}$$

Furthermore,

$$\dot{D}_1(z) = -H(z)(1+z)\frac{dD_1(z)}{dz}\,, \tag{2.18}$$

which is often modeled as $\dot{D}_1(z) = H(z)f(z)D_1(z)$. Within ΛCDM, the function f can be determined analytically from eq. (2.16): it depends only on $\Omega_{\rm m}(z)$ and is well approximated by $f(z) \simeq \Omega_{\rm m}(z)^{0.56}$, see ref. [31]. The amplitude of the power spectrum is given by $A_{\rm s}$ or σ_8^2, which is fixed by $A_{\rm s}$ with a slight dependence on $n_{\rm s}$. We therefore find that, at linear level:

$$P_v(k,z_m,z_n) \propto \begin{cases} f(z_m)f(z_n)H_0^2 A_{\rm s}\,, \text{ or} \\ f(z_m)f(z_n)H_0^2\sigma_8^2\,. \end{cases} \tag{2.19}$$

In the literature it is often assumed that H_0 is known, and the amplitude of the velocity power spectrum is used to determine $f\sigma_8$, see e.g. ref. [19]. Here we proceed in the opposite way: we fix the model to be ΛCDM so that $f(z)$ is given and we use the velocity power spectrum to determine $H_0^2 A_{\rm s}$ (noting that we could also replace $A_{\rm s}$ by σ_8^2). We use the full shape of the velocity power spectrum to calculate the velocity covariance matrix; this depends on H_0 and $\Omega_{\rm m}$ also via the equality scale.

In order to take into account unequal time correlations of the matter power spectrum, we use the approximation described in ref. [33], according to which:

$$P_\delta(k,z_m,z_n) = \mathcal{Z}(k,z_m,z_n)\,P_\delta(k,\bar{z})\,, \tag{2.20}$$

with

$$\mathcal{Z}(k,z_m,z_n) = e^{-(k/k_{\rm NL})^2[D_1(z_m)-D_1(z_n)]^2} \tag{2.21}$$

and the mean redshift $\tilde{z}$ is defined by

$$D_1(z_m)D_1(z_n) = D_1^2(\tilde{z})\,. \tag{2.22}$$

The $\mathcal{Z}(k,z_m,z_n)$ prefactor depends also on the non-linearity scale $k_{\rm NL}$ given by:

$$k_{\rm NL}^{-2} = \frac{1}{12\pi^2}\int_0^\infty P_\delta(k,0)\,{\rm d}k\,. \tag{2.23}$$

Using eq. (2.22), we can rewrite eq. (2.20) as:

$$P_\delta(k,z_m,z_n) = \mathcal{Z}(k,z_m,z_n)\,D_1(z_m)D_1(z_n)P_\delta(k,0)\,. \tag{2.24}$$

Combining everything, we obtain the following expression for the velocity covariance:

$$C^{(\rm v)}_{mn} = \frac{B_{mn}}{2\pi^2}\frac{D_1(z_m)\;D_1(z_n)}{D_1^2(0)}\left[\frac{H(z_m)f(z_m)}{(1+z_m)}\right]\left[\frac{H(z_n)f(z_n)}{(1+z_n)}\right] \int {\rm d}k W_{mn}(k)\mathcal{Z}(k,z_m,z_n)P_\delta(k,0)\,. \tag{2.25}$$

We compute the linear power spectrum using CAMB [34] up to $k_{\rm max} = 100\,h/{\rm Mpc}$.

JCAP09(2025)005

Unlike other works, we do not fix the value of the integral in eq. (2.25) to the one for the fiducial parameters. Rather, we keep the dependence on cosmological parameters inside the integrand, and tackle the expensive integral for each parameter choice and supernovae pair (m, n) with an efficient pipeline, which we describe in section 3. Moreover, in our analysis we have found that the unequal time decoherence factor $\mathcal{Z}(k, z_m, z_n)$ does not significantly impact the results. This is understood by the fact that supernovae that are at sufficiently different redshifts such that $D_1(z_m) - D_1(z_n)$ is appreciable are so far apart that the power spectrum $P_\delta(k)$ is very small for these k values. We note that without $\mathcal{Z}(k, z_m, z_n)$, H_0 and A_s are nearly degenerate in the linear velocity power spectrum, P_v; the degeneracy is in principle lifted by the equality scale.

2.1.1 The non-linear velocity power spectrum

We further consider phenomenological corrections to the linear power spectrum, following refs. [35, 36]. We define the non-linear velocity power spectrum P_v^NL as:

$$P_\mathrm{v}^\mathrm{NL}(k, z_m, z_n) = P_\mathrm{v}(k, z_m, z_n)\, D_\mathrm{u}^2(k\sigma_\mathrm{u})\, E(\sigma_8)\,, \tag{2.26}$$

with

$$D_\mathrm{u}(k\sigma_\mathrm{u}) = \mathrm{sinc}(k\sigma_\mathrm{u}) \tag{2.27}$$

a damping function correction introduced in ref. [35], and $E(\sigma_8)$ an extra non-linear correction with 3% accuracy for $k < 0.7\,h\mathrm{Mpc}^{-1}$ based on ref. [36]:

$$E(\sigma_8) = e^{-k\max\left[a_1(\sigma_8)+a_2(\sigma_8)k+a_3(\sigma_8)k^2,0\right]}\,, \tag{2.28}$$

where the max function has been added to ensure this term is exponentially decaying even for low values of σ_8. We fix $\sigma_\mathrm{u} = 13\ h^{-1}\mathrm{Mpc}$, following ref. [35]. The coefficients a_i are linear functions of the root-mean-square of matter density fluctuations σ_8,

$$a_1(\sigma_8) = (-0.817 + 3.198\,\sigma_8)\,\mathrm{Mpc}/h\,, \tag{2.29}$$

$$a_2(\sigma_8) = (0.877 - 4.191\,\sigma_8)\,\mathrm{Mpc}^2/h^2\,, \tag{2.30}$$

$$a_3(\sigma_8) = (-1.199 + 4.629\,\sigma_8)\,\mathrm{Mpc}^3/h^3\,. \tag{2.31}$$

At fixed n_s, σ_8 is proportional to A_s and given by:

$$\sigma_8 = (\sigma_{8,Planck}\,/A_{\mathrm{s},Planck})A_\mathrm{s}\,,$$

where for $\sigma_{8,Planck} = 0.8102$ and $A_{\mathrm{s},Planck} = 10^{-10}\exp(3.047) = 2.105\times10^{-9}$ we choose the fiducial values from *Planck* (TT,TE,EE+lowE+lensing+BAO) [37]. Furthermore, we set $n_\mathrm{s} = 0.965$ and the baryon density parameter $\omega_\mathrm{b} = 0.02242$. We checked that we obtain consistent results if we assume a higher $\sigma_\mathrm{u} = 21\ h^{-1}\mathrm{Mpc}$, as in refs. [38, 39], and defer an improved modeling of the velocity power spectrum, following e.g. [40], to future work. We show the scaling of the non-linear power spectrum with H_0 and A_s in figure 1.

While the linear velocity power spectrum is proportional to $H_0^2 A_\mathrm{s}$ and therefore H_0 and A_s are degenerate, this is no longer the case in the non-linear power spectrum as $E(\sigma_8)$ depends on A_s but not on H_0. However, as we shall see in section 4, the presently available data still show a severe degeneracy between the value of H_0 inferred from the velocity covariance and A_s.

JCAP09(2025)005

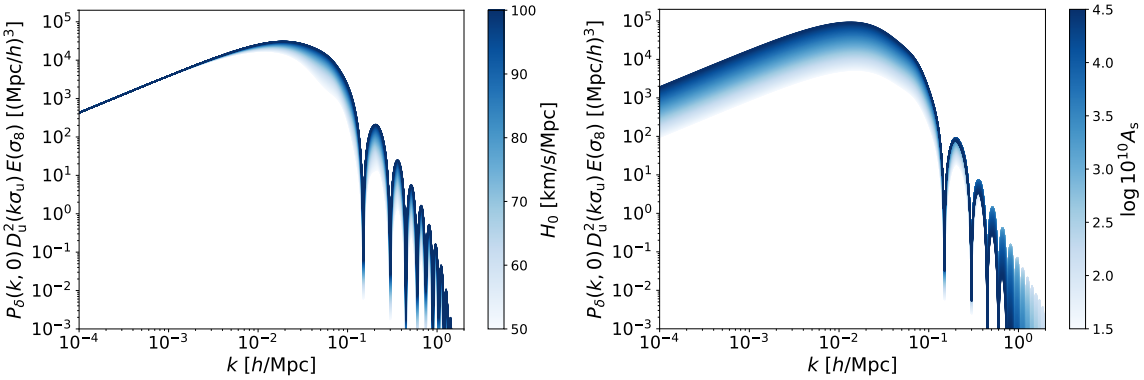

Figure 1. Variation of the non-linear power spectrum we assume in this work with H_0 (left panel) and $\log_{10}(10^{10}A_{\rm s})$ (right panel), with fixed $\log_{10}(10^{10}A_{\rm s}) = 3$ and $H_0 = 70$, respectively.

2.2 Velocity dispersion

The velocity power spectrum gives in principle the non-linear peculiar velocity field as determined with N-body simulations. However, measuring this field with a finite, relatively small number of tracers adds shot noise that can be taken into account as an additional velocity dispersion [41, 42]. We model this in the form:

$$C_{mn}^{(\rm v),\rm disp} = B_{mn}\sigma_{\rm disp}^2\delta_{mn}\,, \tag{2.32}$$

only for those galaxies not hosting a Cepheid. This additional dispersion has also been interpreted as velocities due to virial motions of galaxies in clusters, see ref. [35]. The factor B_{mn} again converts the velocity variance into a magnitude variance. We leave the value of $\sigma_{\rm disp}$ free in our analysis.

3 Methodology

We develop a differentiable Markov chain Monte Carlo (MCMC) pipeline combining efficient emulators and an affine sampler, running on a single graphics processing unit (GPU) and converging 10^5 times faster than traditional approaches. The emulators' ranges are reported in table 1, which also includes the prior ranges for the MCMC analyses.

3.1 Pipeline description

The integral in eq. (2.25) (with $P_{\rm v}$ replaced by the non-linear velocity power spectrum, $P_{\rm v}^{\rm NL}$) is computationally expensive: assuming a dataset containing 10^3 objects, we need to compute it for all $\sim 5\cdot 10^5$ unique pairs of objects in the dataset at each likelihood evaluation. For each choice of cosmological parameters, i.e. for each step of the MCMC, this requires more than half million evaluations of the integral, with the number increasing quadratically with the number of objects in the survey. For this reason, we develop an emulator to evaluate the integral, computing each element of the covariance matrix using a neural network based on the `CosmoPower` emulation framework [43].

We first randomly select one million combinations of redshift pairs and angles from the Pantheon+ dataset, and concatenate them with cosmological parameters sampled uniformly

JCAP09(2025)005

Parameter	$\Omega_{\rm m}$	H_0	$\log\left(10^{10}A_{\rm s}\right)$	$\log_{10}(\sigma^2_{\rm disp})$	δM
Prior range	$\mathcal{U}[0.1, 0.5]$	$\mathcal{U}[50, 100]$	$\mathcal{U}[1.5, 4.5]$	$\mathcal{U}[2, 6]$	$\mathcal{U}[-0.5, 0.5]$

Table 1. Prior distributions of the parameters for the training of the emulator (first three columns), and for inference (all columns). Uniform distributions are indicated with $\mathcal{U}$. The units of H_0 are km/s/Mpc, while the units of $\sigma_{\rm disp}$ are km/s.

from the ranges indicated in table 1, which also act as the priors for the inference step. We compute the value of the integral using the `FFTLog` algorithm to account for the Bessel functions [44, 45],[4] separating between the case $\alpha_{mn} = 0$ (which does not involve Bessel integrals) and $\alpha_{mn} \neq 0$. We then train two emulators (one for $\alpha_{mn} = 0$ and one for $\alpha_{mn} \neq 0$) to predict the value of the integral given the values of z_1, z_2, α_{12}, $\Omega_{\rm m}$, H_0 and $\log\left(10^{10}A_{\rm s}\right)$, using a mean absolute error loss function to be robust to outliers. We find that each emulator converges in a few hours on a single GPU with a median performance at the sub-percent level on held-out test data, so we are confident that its predictions are accurate. We note that our emulators are trained on redshifts and angles drawn from the Pantheon+ dataset, so in principle one would need to train again in case a new dataset is considered; however, we tested that the performance was still satisfactory even on the N-body simulation data we consider in this paper. In future work, we will explore a more general emulator trained on a uniform distribution of redshifts and angles, which should be applicable to a wider variety of datasets.

We write the likelihood in eq. (2.1) using `JAX` [46, 47], a library that enables differentiable and efficient `Python` code optimized for GPUs. To sample the posterior distribution, we use the `JAX` version of `affine`,[5] a parallelized affine-invariant sampler based on `emcee` [48, 49]; our `CosmoPower` emulator is integrated into the likelihood through `CosmoPower-JAX` [50].[6] The combination of a parallelized sampler and a neural network emulator, both running on a GPU, significantly accelerates our analysis: we sample the posterior distribution for a single model using 22 walkers (18 in the N-body simulation case) and 5000 steps in no more than one hour using a single A100 80GB GPU after training the emulator, which is done once and requires a single day including the generation of the training set. We extrapolate that a similar analysis employing 32 CPUs and no emulator would require ~ 25 years, since each likelihood call requires the evaluation of the integral in eq. (2.25) for each pair of supernovae. For our $\sim 10^6$ pairs this takes about 2 days. This means that the use of our differentiable pipeline provides a total speed-up greater than 10^5. We make our emulator and likelihood codes publicly available.[7]

The MCMC convergence is achieved when the number of steps $N > 50\tau_{\rm max}$, with $\tau_{\rm max}$ the largest integrated autocorrelation time τ among all the parameters (see ref. [49] for more details). After convergence, we discard $2\lfloor\tau_{\rm max}\rfloor$ steps from the chain as burn-in [51]. The contour plots are obtained using `chainconsumer v0.34` [52]. We also verified our MCMC results against a profile likelihood approach [53], finding consistent results.

[4] https://github.com/xfangcosmo/FFTLog-and-beyond.
[5] https://github.com/justinalsing/affine.
[6] https://github.com/dpiras/cosmopower-jax.
[7] https://github.com/dpiras/veloce.

JCAP09(2025)005

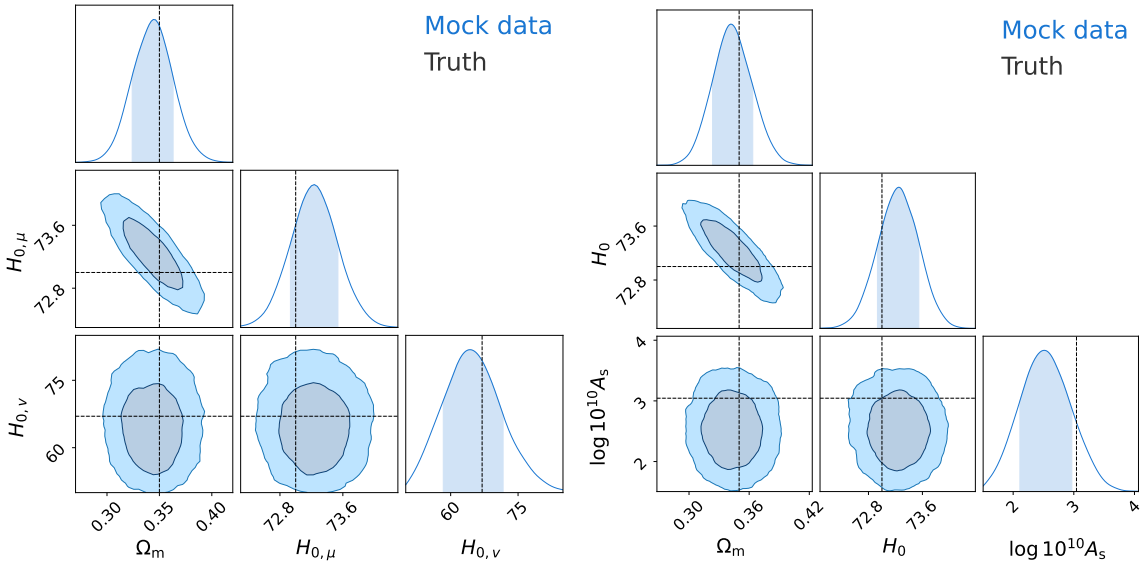

Figure 2. Posterior distribution for the mock test, with the bands indicating the 68% and 95% credible intervals. In the left panel we choose $H_{0,\mu} = 73\,\mathrm{km/s/Mpc}$ for the distances and $H_{0,\mathrm{v}} = 67\,\mathrm{km/s/Mpc}$ for the velocity power spectrum; additionally, $\Omega_\mathrm{m} = 0.35$ and $\log_{10}(10^{10} A_\mathrm{s}) = 3.047$. For the analysis in the right panel we assume $H_{0,\mu} = H_{0,\mathrm{v}}$, but vary A_s which is degenerate with $H_{0,\mathrm{v}}$. We do not include Cepheids in these mock datasets, and simply set $\delta\mathrm{M} \equiv 0$ which leads to an artificially small error in $H_{0,\mu}$. In all figures throughout the paper, H_0 values are in units of km/s/Mpc.

4 Results

4.1 Mock dataset

We generate a mock dataset following the steps described in appendix C. This dataset is modeled with redshifts affected by velocities generated from the velocity covariance matrix in eq. (2.10), and distance moduli with errors given by $C^{(\mathrm{e})}$ as in Pantheon+. In order to study how well we can recover H_0 from the peculiar velocities and from the distance moduli, we choose different input values of H_0 for the velocity covariance, denoted $H_{0,\mathrm{v}} = 67\,\mathrm{km/s/Mpc}$, and the distance modulus, denoted $H_{0,\mu} = 73\,\mathrm{km/s/Mpc}$. As a first step with this mock data, we do not add a velocity dispersion as described in section 2.2, which is present not only in real data but also in N-body simulations.

When fixing A_s, we can recover both $H_{0,\mathrm{v}}$ and $H_{0,\mu}$ within 1σ, as we show in the left panel of figure 2. In the right-hand side plot of figure 2, using the same dataset, we assume just one physical value of $H_0 = H_{0,\mu} = H_{0,\mathrm{v}}$: since the velocity covariance was generated with a different value of H_0 this reproduces now a smaller value of A_s with an only very little increase in goodness of fit ($\log \mathcal{L} = 743$ vs 740). As expected within linear perturbation theory, the result mainly depends on $H_0^2 A_\mathrm{s}$ and a 10% increase in H_0 can be compensated with an about 20% decrease in A_s. We also see that mapping the redshift error onto the magnitude error does not induce a bias in the analysis of the mock dataset, although for larger datasets a more involved analysis may be necessary [54].

JCAP09(2025)005

4.2 *N*-body simulation

As a more realistic test dataset, we use a subset of the simulated distances created by the relativistic N-body code `gevolution` [55] to study the impact of cosmic structure on the Hubble diagram in ref. [56]. For this, a relativistic ray-tracing through the simulation volume has been performed. The simulation covers a cosmological volume of $(2.4\,\mathrm{Gpc}/h)^3$, the metric is sampled on a regular grid of 7680^3 points and the matter density is followed by 7680^3 mass elements. The simulation assumes a flat ΛCDM cosmology with $H_0 = 67.556\,\mathrm{km/s/Mpc}$, $\Omega_\mathrm{m} = 0.312046$ and $A_\mathrm{s} = 2.215\times10^{-9}$, corresponding to $\log 10^{10} A_\mathrm{s} = 3.098$. The lightcone was recorded on a circular pencil beam covering $450\,\mathrm{deg}^2$. More details can be found in ref. [56].

These N-body distances contain the velocity and lensing contributions by construction, but have essentially vanishing intrinsic scatter. To make them more realistic, we add random noise to the data with a given constant standard deviation $\sigma_0 = 0.03$, roughly corresponding to one order of magnitude less than Pantheon+, to test a scenario with smaller error bars corresponding to a higher number of SNIa.[8] We then write the error covariance matrix as:

$$C^{(\mathrm{e})}_{mn} = \left(\sigma_0^2 + \sigma_l^2 z^2\right)\delta_{mn}$$

for the chosen value of σ_0 and for a lensing contribution of $\sigma_l = 0.055$ [57]. To this we add the velocity covariance $C^{(\mathrm{v})}_{mn}$ and the velocity dispersion $C^{(\mathrm{v}),\mathrm{disp}}_{mn}$ as described in section 2.

From the large number of distances to halos available in this data set, we randomly select 1701 halos in the redshift range $[0.01, 1]$ with a redshift distribution similar to the one of the Pantheon+ data. Given the box size and resolution, we expect that the large-scale structure is correctly resolved down to significantly smaller redshifts. We also have checked that the monopole, dipole and quadrupole contributions to the luminosity distance are negligible in this near 'pencil beam' data.

We perform the same analyses with the N-body simulations as in the next section for the real supernova data. We first fix A_s and assume two different values of H_0, one for the distance modulus, $H_{0,\mu}$, and one for the peculiar velocities, $H_{0,\mathrm{v}}$. The results, shown in the left panel of figure 3, indicate that we manage to recover Ω_m and both H_0 values within 1σ, with a velocity dispersion of $\sigma_\mathrm{disp} = 155^{+18}_{-16}\,\mathrm{km/s}$. In the right panel of figure 3 we further show that, assuming a single H_0, we also retrieve the correct value of $\log 10^{10} A_\mathrm{s}$, with a consistent value of σ_disp.

In figure 4 we show the results of a parameter estimation mimicking an analysis without any Cepheid anchors. Clearly, the degeneracy between H_0 and the distance shift $\delta\mathrm{M}$ is considerable, but it is partially broken by the velocity covariance, allowing us to recover well the input value of H_0, for which we find $H_0 = 71.4^{+4.7}_{-4.6}\,\mathrm{km/s/Mpc}$. The input Ω_m is also well recovered, while the required velocity dispersion of $\sigma_\mathrm{disp} = 155^{+18}_{-16}\,\mathrm{km/s}$ is in good agreement with the Pantheon+ data results discussed below. While the non-linear corrections in the velocity covariance matrix can in principle break the degeneracy between A_s and H_0, we still find in this analysis a strong degeneracy, namely we can either determine H_0

[8] Assuming the true intrinsic spread is 0.1 mag but uncorrelated for different supernovae (in different galaxies), then multiplying the observed number of supernovae by a factor 10 would correspond roughly to a reduction of the statistical part of the standard deviation by a factor $\sqrt{10} \simeq 3$; this translates into an intrinsic magnitude reduction from 0.1 mag to about 0.03 mag.

JCAP09(2025)005

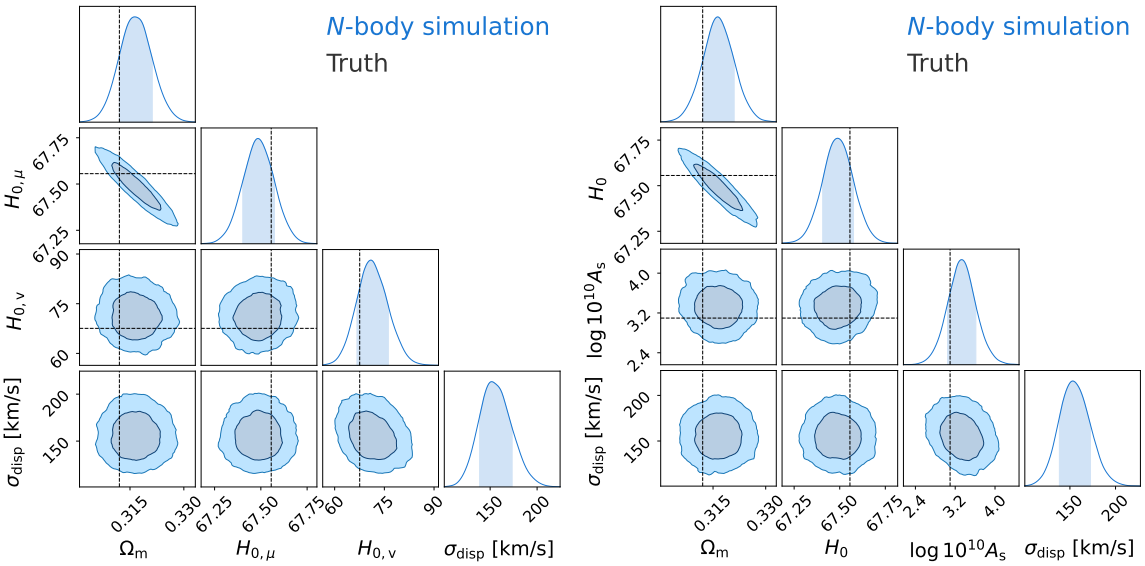

Figure 3. Results from the N-body simulation run with `gevolution`. The blue contours indicate the 68% and 95% credible intervals, while the black dashed lines represent the input cosmological parameters for the N-body simulation. The left panel shows that, given A_s, we can determine H_0 either via the distance moduli, $H_{0,\mu}$ or via the peculiar velocity covariance, $H_{0,v}$. In the right panel, we consider only one value of $H_0 = H_{0,\mu} = H_{0,v}$, and we use the velocity covariance to determine A_s.

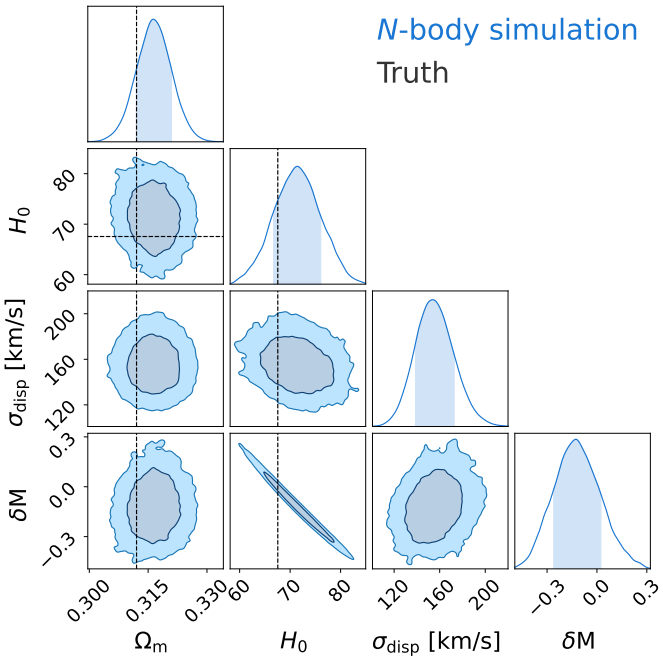

Figure 4. Results from the N-body simulation `gevolution` 'without cepheids', namely with δM acting as calibration parameter. The blue contours indicate the 68% and 95% credible intervals, while the input cosmological parameters for the N-body simulation are shown as dashed lines. Fixing A_s to the input value, we use the velocity covariance to determine H_0 without the help of anchors. The degeneracy with δM, while not being completely lifted, is significantly reduced.

JCAP09(2025)005

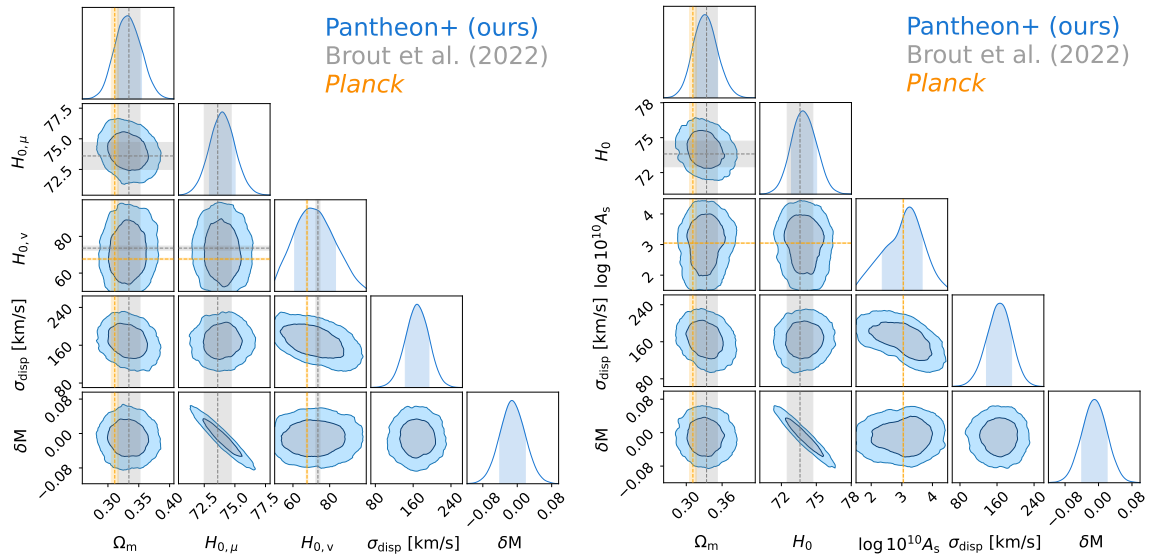

Figure 5. 68% and 95% posterior contours from the Pantheon+ data including Cepheid information. In the left panel, we model the peculiar velocities with fixed (A_s, n_s) from the *Planck* data, and fit H_0 from the distance moduli ($H_{0,\mu}$) and from the velocity covariance ($H_{0,v}$) independently. The inferred value for $H_{0,v}$ has large error bars and cannot distinguish between the value inferred from the traditional supernova analysis (gray bands) and the *Planck* value (orange bands). In the right panel, we model the data with one value for H_0 and use the velocity covariance to determine A_s. Again, the errors are still rather large with present data, but demonstrate the potential of our approach.

or A_s, but not both at the same time. This might be due to the fact that there are very few nearby supernovae in this dataset, so that the non-linear corrections to the velocity covariance are not very important here. We will however always show results including the non-linear modeling of the velocity covariance.

4.3 Pantheon+ data

As in our previous analyses (see refs. [29, 58, 59]), we use the Pantheon+SH0ES dataset providing 1701 lightcurves [4, 26]; of these, 77 SNIa are in galaxies hosting Cepheids, whose absolute distance modulus μ_{ceph} is known. For the analysis of the Pantheon+ data, we start from the Pantheon+ covariance matrix with the statistical and systematic contributions from peculiar velocities subtracted, and we add our peculiar velocity covariance matrix $C^{(v)}_{mn}$. When fixing A_s and n_s to the *Planck* values, the velocity covariance matrix depends on H_0 and Ω_m via the power spectrum P_v. We first fix A_s to the *Planck* value and allow for an independent H_0 for both the distance modulus, $H_{0,\mu}$ and the velocity covariance, $H_{0,v}$; the result is shown in the left panel of figure 5. Clearly, $H_{0,v}$ has very wide contours and cannot distinguish between the values preferred by the distance Pantheon+ data [4] (gray bands) and the *Planck* data [37] (orange bands). On the other hand, we can use the distance moduli and the velocity covariance to jointly model the value of H_0, Ω_m and A_s, which we show in the right panel of figure 5. In this way, supernovae provide an independent value of the scalar perturbation amplitude A_s which is nearly independent of *Planck* data (only the value n_s is adopted from *Planck*).

JCAP09(2025)005

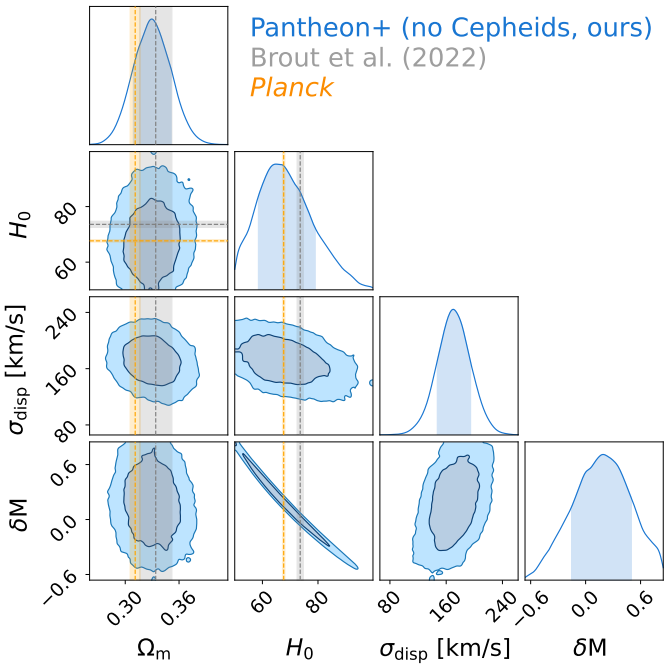

Figure 6. 68% and 95% posterior contours from the Pantheon+ analysis without using Cepheid anchors. The degeneracy between δM and H_0 is broken only by our treatment of the velocity covariance. The *Planck* values for H_0 and $\Omega_{\rm m}$ are indicated as orange bands, while in gray we report the values from the latest Pantheon+ analysis [4].

Analysis	$H_{0,\mu}$ [km/s/Mpc]	$H_{0,\rm v}$ [km/s/Mpc]	$\log 10^{10} A_{\rm s}$	$\sigma_{\rm disp}$ [km/s]	δM
With Cepheids, fixed $A_{\rm s}$ (figure 5)	$74.0^{+1.0}_{-1.0}$	$72.0^{+12.0}_{-11.0}$	-	169^{+25}_{-25}	$-0.01^{+0.03}_{-0.03}$
With Cepheids, free $A_{\rm s}$ (figure 5)	$73.9^{+1.1}_{-1.1}$	-	$3.1^{+0.5}_{-0.8}$	165^{+26}_{-28}	$-0.01^{+0.03}_{-0.03}$
No Cepheids, fixed $A_{\rm s}$ (figure 6)	$67.7^{+11.3}_{-9.2}$	-	-	171^{+24}_{-24}	$0.18^{+0.32}_{-0.34}$

Table 2. Parameter constraints (median ± 68% credible intervals) for the Pantheon+ analyses, with all details available in section 4.3. All analyses find $\Omega_{\rm m} = 0.33 \pm 0.02$. We have $H_{0,\mu} = H_0$ in the second and third rows.

We finally remove the calibrators from the Pantheon+ dataset and perform an analysis assuming a single H_0 while fixing $A_{\rm s}$ to its *Planck* value. In this instance only, we extend the δM prior range to $[-1, 1]$. The results, presented in figure 6. cannot yet distinguish between the *Planck* value and the value from the standard SNIa analysis; however, we start breaking the degeneracy between H_0 and δM, finding:

$$H_0 = 67.7^{+11.3}_{-9.2}\,\text{km/s/Mpc}\,.$$

All numerical results for our Pantheon+ analyses are presented in table 2.

JCAP09(2025)005

5 Conclusions

In this paper, we introduce a novel method to use SNIa peculiar velocities to constrain cosmological parameters without the need for anchors such as the Cepheids, by exploiting the H_0 dependence of the covariance matrix of the peculiar velocities. So far, our analysis constrains either A_s or the Hubble parameter in the velocity power spectrum, $H_{0,\mathrm{v}}$, since the linear velocity power spectrum only depends on the product $H_0^2 A_\mathrm{s}$. With more low redshift supernovae, we shall also become more sensitive to non-linear corrections which break this degeneracy. We developed an efficient differentiable pipeline and validated our approach on mock datasets and on N-body simulations. We then applied it to the Pantheon+ data, finding that $H_{0,\mathrm{v}} = 72.0^{+12.0}_{-11.0}\,\mathrm{km/s/Mpc}$ for the double H_0 analysis, while for the single H_0 analysis without Cepheids we find $H_0 = 67.7^{+11.3}_{-9.2}\,\mathrm{km/s/Mpc}$.

Our work showcases a new path to address tensions between early and late Universe probes [60]. Presently, there is a considerable debate concerning the use of anchors for supernova measurements [61–63]; our method is independent of these anchors, depending only on the peculiar velocity power spectrum. While present data does not have sufficiently many low redshift supernova to allow a precise measurement of the velocity power spectrum, the proposed method will achieve its full potential with upcoming surveys like ZTF [20] and the Vera Rubin Legacy Survey of Space and Time (LSST, [64]), providing significantly more data especially at low redshift. As peculiar velocities contribute most to the Hubble diagram at low redshifts, especially in the analysis of ZTF with an order of magnitude more supernovae with redshifts $z < 0.1$, our method promises to unlock precise cosmological constraints without relying on anchors.

We plan to extend our analysis in several ways. For instance, we will implement a differentiable version of the low multipoles of the luminosity distance, based on ref. [29], which will allow us to jointly sample the multipoles and the cosmological parameters. We will also implement other contributions to the peculiar velocities, such as the vorticity power spectrum. Vorticity is usually neglected when modeling velocities; nevertheless, some works (e.g. [65]) have shown that it is an important contribution to the velocity power spectrum at late time, exactly when peculiar velocities become more and more relevant in the Hubble diagram. We will also further evaluate the robustness of our new implementations with more refined N-body simulations.

Most importantly, we plan to apply our routine to larger supernova datasets as the LSST and, in particular, the ZTF. The contribution from ZTF will be particularly relevant since it is expected to observe many supernovae at low redshift; for example, the upcoming Data Release 2.5 is anticipated to contain thousands of objects at $z \leq 0.3$ [23]. In order to obtain competitive constraints which can distinguish between the presently advocated values of H_0, we will need about 10 times more SNIa at low redshift ($z \lesssim 0.1$) than the present dataset; Pantheon+ contains 664 SNIa with $z < 0.1$, excluding the 77 SNIa in galaxies hosting Cepheids. In our upcoming analyses, we will expand our pipeline to jointly fit the covariance matrix along with the parameters of the Tripp formula [66], as well as to include selection and systematic effects such as Malmquist bias and chromatic intrinsic scatter. Our approach can also be modified to work with other distance relations like the Tully-Fisher relation [67] and the Fundamental Plane relation [68, 69], as well as to be applied to datasets like CosmicFlows-4 [70], containing distances to 55877 galaxies collected into 38065 groups.

JCAP09(2025)005

6 Data availability

The Pantheon+ dataset and distance modulus covariances are available in the official repository https://github.com/PantheonPlusSH0ES/DataRelease. The data and the code to reproduce our analysis, together with the emulator for the velocity covariance power spectrum, will be made public upon acceptance of this paper at this GitHub repository: https://github.com/dpiras/veloce.

Acknowledgments

We thank Anthony Carr, Richard Watkins, Pedro Ferreira and Alex Kim for useful discussions; in particular, we would like to thank Anthony Carr for sharing the Pantheon+ covariance without the peculiar velocity contribution. DP, FS and MK acknowledge financial support from the Swiss National Science Foundation. DP was additionally supported by the SNF Sinergia grant CRSII5-193826 "AstroSignals: A New Window on the Universe, with the New Generation of Large Radio-Astronomy Facilities". The computations underlying this work were performed on the Baobab cluster at the University of Geneva. This work used data originally generated by a grant from the Swiss National Supercomputing Centre (CSCS) under project ID s710.

A Derivation of δz

We assume that the shift in $\bar{z} = z + \delta z_i$ due to the peculiar velocity of supernova i is small, so that we can write:

$$\mu(\bar{z}_i) = \mu(z_i) + \mu'(z_i)\delta z_i\,, \quad \delta z_i = \frac{v_i/c}{1+z_i}\,, \tag{A.1}$$

where $v_i = \mathbf{v}(\mathbf{n}_i, z_i)\cdot\mathbf{n}_i$ is the radial peculiar velocity of supernova i,[9] and $\mathbf{n}_i$ its position. The derivative of the distance modulus $\mu = 5\log_{10}(d_\mathrm{L}/1\mathrm{Mpc}) + 25$ is given by

$$\mu'(z_i) = \frac{\partial\mu}{\partial z_i} = \frac{5}{\log(10)}\frac{d'_\mathrm{L}(z_i)}{d_\mathrm{L}(z_i)}\,. \tag{A.2}$$

We can invert the relation to obtain the shift in z:

$$\delta z_i = \frac{\mu(\bar{z}_i) - \mu(z_i)}{\mu'(z_i)} = \frac{\log(10)}{5}\frac{d_\mathrm{L}(z_i)}{d'_\mathrm{L}(z_i)}\left[\mu(\bar{z}_i) - \mu(z_i)\right]\,. \tag{A.3}$$

From the definition of the background $d_\mathrm{L}(z)$ we have that:

$$\frac{d'_\mathrm{L}}{d_\mathrm{L}} = \frac{1}{1+z} + \frac{1+z}{H(z)d_\mathrm{L}(z)} = \frac{1}{1+z}\left(1 + \frac{(1+z)^2}{H(z)d_\mathrm{L}(z)}\right)\,. \tag{A.4}$$

Furthermore, also $d_\mathrm{L}(\bar{z})$ is proportional to the source frequency squared, adding a term $-2\delta z/(1+z)d_\mathrm{L}$ which inverts the sign of the first term in the final expression (see ref. [27]

[9] We neglect corrections in the redshift due to the gravitational field which are usually much smaller.

JCAP09(2025)005

for a detailed derivation including also the gravitational terms). Using the peculiar velocity term of ref. [27] in the equation for δz and writing $\delta\mu^{(v)} = \mu(\bar{z}) - \mu(z)$, we find:

$$\delta z_i = \frac{\log(10)}{5}\delta\mu_i^{(v)}\frac{1+z_i}{\frac{c(1+z_i)^2}{H(z_i)d_{\rm L}(z_i)}-1}\,, \tag{A.5}$$

or equivalently

$$v_i = \frac{\log(10)}{5}\delta\mu_i^{(v)}\frac{c}{\frac{c(1+z_i)^2}{H(z_i)d_{\rm L}(z_i)}-1}\,, \tag{A.6}$$

which agrees with eq. (2.9).

B Derivation of the window function

To calculate the window function as in eq. (2.13), we must determine the integrals:

$$W_{mn}(k) = \sum_{i,j=1}^{3}\mathbf{n}_{m,i}\mathbf{n}_{n,j}\int\frac{{\rm d}\Omega_{\hat{k}}}{4\pi}\hat{\mathbf{k}}_i\,\hat{\mathbf{k}}_j e^{ik\hat{\mathbf{k}}\cdot(\mathbf{r}_m-\mathbf{r}_n)} = \sum_{ij}\mathbf{n}_{m,i}\mathbf{n}_{n,j}W_{mnij}(k)\,, \tag{B.1}$$

where $\mathbf{n}_m = \mathbf{r}_m/r_m$ and $\mathbf{n}_n = \mathbf{r}_n/r_n$ are the directions of the m-th and n-th SNIa respectively. To simplify the calculation we orient the coordinate system in $\mathbf{k}$-space such that $\mathbf{r}_m - \mathbf{r}_n$ is in the z-direction, and both $\mathbf{r}_m$ and $\mathbf{r}_n$ are in the $\varphi = 0$ plane; hence $r_{m2} = r_{n2} = 0$. Furthermore, it is easy to see that the φ-integral of $W_{mnij}(k)$ vanishes whenever $i \neq j$. Using $\cos\theta = \mu$ such that ${\rm d}\Omega_{\hat{k}} = \sin\theta d\theta d\varphi = d\mu d\varphi$ and setting $|\mathbf{r}_m - \mathbf{r}_n| = R_{mn}$, we obtain:

$$\begin{aligned} W_{mn33}(k) &= \frac{1}{2}\int_{-1}^{1}\mu^2 e^{ikR_{mn}\mu} \\ &= \frac{2kR_{mn}\cos(kR_{mn}) + ((kR_{mn})^2-2)\sin(kR_{mn})}{(kR_{mn})^3}\,, \end{aligned} \tag{B.2}$$

$$\begin{aligned} W_{mn11}(k) &= \frac{1}{4\pi}\int_0^{2\pi}\cos^2\varphi\int_{-1}^{1}(1-\mu^2)e^{ikR_{mn}\mu} \\ &= \frac{-2kR_{mn}\cos(kR_{mn}) + 2\sin(kR_{mn})}{(kR_{mn})^3}\,. \end{aligned} \tag{B.3}$$

We now use that:

$$W_{mn}(k) = (n_{m3}n_{n3} + n_{m1}n_{n1})W_{mn33} + n_{m1}n_{n1}(W_{mn11} - W_{mn33})\,.$$

Furthermore, one easily verifies that:

$$W_{mn33}(k) = \frac{1}{3}(j_0(kR_{mn}) - 2j_2(kR_{mn}))$$

and

$$W_{mn11}(k) - W_{mn33}(k) = j_2(kR_{mn})\,.$$

We use also that:

$$n_{m3}n_{n3} + n_{m1}n_{m1} = \cos\alpha_{mn}\,,$$

JCAP09(2025)005

and the elementary triangle relation

$$\frac{\sin\theta_m}{r_n} = \frac{\sin\theta_n}{r_m} = \frac{\sin\alpha_{mn}}{R_{mn}}\,,$$

which implies

$$n_{m1} = \sin\theta_m = r_n \frac{\sin\alpha_{mn}}{R_{mn}}$$

and

$$n_{n1} = \sin\theta_n = r_m \frac{\sin\alpha_{mn}}{R_{mn}}\,.$$

Putting it all together we arrive at the final result:

$$W_{mn}(k) = \frac{1}{3}\cos\alpha_{mn}(j_0(kR_{mn}) - 2j_2(kR_{mn})) + \frac{r_m r_n}{R_{mn}^2} j_2(kR_{mn})\sin^2\alpha_{mn}\,. \tag{B.4}$$

C Mock dataset

For the sake of simplicity and to avoid numerical instabilities, we create our mock dataset starting from a subset of Pantheon+ without Cepheids containing 1457 individual lightcurves. These are obtained by iteratively removing the element corresponding to the largest absolute component of the eigenvector associated with the most negative eigenvalue, until the resulting velocity covariance matrix is semi-positive definite. We correspondingly subsample the error covariance $C^{(\mathrm{e})}_{mn}$ obtained from the full Pantheon+ covariance. This procedure is necessary due to the presence of objects with similar, or even identical, sky position in the Pantheon+ collection, which make the Cholesky decomposition in eq. (C.3) unfeasible.

We choose the heliocentric redshifts of the original dataset as background redshift $\bar{z}$ of the mock dataset. We then define the mock observed redshifts z_i^{mock} for the i-th object as:

$$z_i^{\mathrm{mock}} = \bar{z}_i + \delta z_i\,, \tag{C.1}$$

with the peculiar velocity contribution

$$\delta z_i = \sum_j D_{ij} g_j\,. \tag{C.2}$$

Here, g_j is sampled from a Gaussian distribution with mean 0 and variance 1, while D_{ij} is obtained from the Cholesky decomposition of our velocity covariance:

$$\frac{C^{(\mathrm{v}),\mathrm{z}}}{c^2} = DD^{\mathrm{T}}, \tag{C.3}$$

with c being the speed of light and

$$C^{(\mathrm{v}),\mathrm{z}} = C^{(\mathrm{v}),\mathrm{v}}(1+z_m)(1+z_n). \tag{C.4}$$

$C^{(\mathrm{v}),\mathrm{v}}$ is the covariance in eq. (2.10) obtained assuming $H_{0,\mathrm{v}} = 67\,\mathrm{km/s/Mpc}$, $\Omega_{\mathrm{m}} = 0.35$ and $\log_{10}(10^{10}A_{\mathrm{s}}) = 3.04$. Finally, we define the mock distance modulus as:

$$\mu_i^{\mathrm{mock}} = \mu_i(\bar{z}_i) + h_i\,\sigma_i^{\mu} \tag{C.5}$$

with h_i sampled from a Gaussian distribution with mean 0 and variance 1, and $(\sigma_i^{\mu})^2$ is the i-th element of the diagonal of the Pantheon+ covariance without peculiar velocity correction. $\mu_i(\bar{z}_i)$ is obtained from eq. (2.3) assuming the same cosmology as for z_i^{mock} except for $H_{0,\mu} = 73\,\mathrm{km/s/Mpc}$.

JCAP09(2025)005

References

[1] Supernova Search Team collaboration, *The High Z supernova search: Measuring cosmic deceleration and global curvature of the universe using type Ia supernovae*, *Astrophys. J.* **507** (1998) 46 [astro-ph/9805200] [INSPIRE].

[2] Supernova Search Team collaboration, *Observational evidence from supernovae for an accelerating universe and a cosmological constant*, *Astron. J.* **116** (1998) 1009 [astro-ph/9805201] [INSPIRE].

[3] Supernova Cosmology Project collaboration, *Measurements of Ω and Λ from 42 High Redshift Supernovae*, *Astrophys. J.* **517** (1999) 565 [astro-ph/9812133] [INSPIRE].

[4] D. Brout et al., *The Pantheon+ Analysis: Cosmological Constraints*, *Astrophys. J.* **938** (2022) 110 [arXiv:2202.04077] [INSPIRE].

[5] A. Carr et al., *The Pantheon+ analysis: Improving the redshifts and peculiar velocities of Type Ia supernovae used in cosmological analyses*, *Publ. Astron. Soc. Austral.* **39** (2022) e046 [arXiv:2112.01471] [INSPIRE].

[6] E. Tsaprazi and A.F. Heavens, *Field-level inference of H_0 from simulated type Ia supernovae in a local Universe analogue*, *Mon. Not. Roy. Astron. Soc.* **539** (2025) 1448 [arXiv:2502.08385] [INSPIRE].

[7] T.M. Davis et al., *The Effect of Peculiar Velocities on Supernova Cosmology*, *Astrophys. J.* **741** (2011) 67 [arXiv:1012.2912] [INSPIRE].

[8] G. Efstathiou, *To H0 or not to H0?*, *Mon. Not. Roy. Astron. Soc.* **505** (2021) 3866 [arXiv:2103.08723] [INSPIRE].

[9] A.G. Riess et al., *A Comprehensive Measurement of the Local Value of the Hubble Constant with 1 km s^{-1} Mpc^{-1} Uncertainty from the Hubble Space Telescope and the SH0ES Team*, *Astrophys. J. Lett.* **934** (2022) L7 [arXiv:2112.04510] [INSPIRE].

[10] CosmoVerse Network collaboration, *The CosmoVerse White Paper: Addressing observational tensions in cosmology with systematics and fundamental physics*, *Phys. Dark Univ.* **49** (2025) 101965 [arXiv:2504.01669] [INSPIRE].

[11] E. Macaulay et al., *Power Spectrum Estimation from Peculiar Velocity Catalogues*, *Mon. Not. Roy. Astron. Soc.* **425** (2012) 1709 [arXiv:1111.3338] [INSPIRE].

[12] H.A. Feldman, R. Watkins and M.J. Hudson, *Cosmic Flows on 100 h^{-1} Mpc Scales: Standardized Minimum Variance Bulk Flow, Shear and Octupole Moments*, *Mon. Not. Roy. Astron. Soc.* **407** (2010) 2328 [arXiv:0911.5516] [INSPIRE].

[13] A. Johnson et al., *The 6dF Galaxy Survey: cosmological constraints from the velocity power spectrum*, *Mon. Not. Roy. Astron. Soc.* **444** (2014) 3926 [arXiv:1404.3799] [INSPIRE].

[14] L.A. Campbell et al., *The 6dF Galaxy Survey: Fundamental Plane Data*, *Mon. Not. Roy. Astron. Soc.* **443** (2014) 1231 [arXiv:1406.4867] [INSPIRE].

[15] C. Howlett et al., *2MTF — VI. Measuring the velocity power spectrum*, *Mon. Not. Roy. Astron. Soc.* **471** (2017) 3135 [arXiv:1706.05130] [INSPIRE].

[16] K.L. Masters, C.M. Springob and J.P. Huchra, *2MTF I. The Tully-Fisher Relation in the 2MASS J, H and K Bands*, *Astron. J.* **135** (2008) 1738 [arXiv:0711.4305] [INSPIRE].

[17] D. Huterer, D.L. Shafer, D.M. Scolnic and F. Schmidt, *Testing ΛCDM at the lowest redshifts with SN Ia and galaxy velocities*, *JCAP* **05** (2017) 015 [arXiv:1611.09862] [INSPIRE].

JCAP09(2025)005

[18] D. Scolnic et al., *Supercal: cross-calibration of multiple photometric systems to improve cosmological measurements with type ia supernovae*, *Astrophys. J.* **815** (2015) 117 [arXiv:1508.05361] [INSPIRE].

[19] B. Carreres et al., *Growth-rate measurement with type-Ia supernovae using ZTF survey simulations*, *Astron. Astrophys.* **674** (2023) A197 [arXiv:2303.01198] [INSPIRE].

[20] E.C. Bellm et al., *The Zwicky Transient Facility: System Overview, Performance, and First Results*, *Publ. Astron. Soc. Pac.* **131** (2018) 018002 [arXiv:1902.01932].

[21] C. Ravoux et al., *Generalized framework for likelihood-based field-level inference of growth rate from velocity and density fields*, *Astron. Astrophys.* **698** (2025) A273 [arXiv:2501.16852] [INSPIRE].

[22] B. Carreres et al., *ZTF SN Ia DR2: Peculiar velocities' impact on the Hubble diagram*, *Astron. Astrophys.* **694** (2025) A8 [arXiv:2405.20409] [INSPIRE].

[23] M. Rigault et al., *ZTF SN Ia DR2: Overview*, *Astron. Astrophys.* **694** (2025) A1 [arXiv:2409.04346] [INSPIRE].

[24] A.M. Hollinger and M.J. Hudson, *Uncertainties in the Hubble constant from peculiar velocities*, *JCAP* **08** (2025) 021 [arXiv:2501.15704] [INSPIRE].

[25] A. Abate and O. Lahav, *The Three Faces of Ω_m: Testing Gravity with Low and High Redshift SN Ia Surveys*, *Mon. Not. Roy. Astron. Soc.* **389** (2008) 47 [arXiv:0805.3160] [INSPIRE].

[26] D. Scolnic et al., *The Pantheon+ Analysis: The Full Data Set and Light-curve Release*, *Astrophys. J.* **938** (2022) 113 [arXiv:2112.03863] [INSPIRE].

[27] C. Bonvin, R. Durrer and M.A. Gasparini, *Fluctuations of the luminosity distance*, *Phys. Rev. D* **73** (2006) 023523 [*Erratum ibid.* **85** (2012) 029901] [astro-ph/0511183] [INSPIRE].

[28] M. Pantiri, M. Foglieni, E. Di Dio and E. Castorina, *The power spectrum of luminosity distance fluctuations in General Relativity*, *JCAP* **11** (2024) 021 [arXiv:2407.01486] [INSPIRE].

[29] F. Sorrenti, R. Durrer and M. Kunz, *The low multipoles in the Pantheon+SH0ES data*, *JCAP* **04** (2025) 013 [arXiv:2403.17741] [INSPIRE].

[30] Y.-Z. Ma, C. Gordon and H.A. Feldman, *The peculiar velocity field: constraining the tilt of the Universe*, *Phys. Rev. D* **83** (2011) 103002 [arXiv:1010.4276] [INSPIRE].

[31] EUCLID collaboration, *Euclid preparation — XL. Impact of magnification on spectroscopic galaxy clustering*, *Astron. Astrophys.* **685** (2024) A167 [arXiv:2311.03168] [INSPIRE].

[32] M. Abramowitz and I. Stegun, *Handbook of Mathematical Functions*, Dover Publications, New York, U.S.A. (1972).

[33] N.E. Chisari and A. Pontzen, *Unequal time correlators and the Zel'dovich approximation*, *Phys. Rev. D* **100** (2019) 023543 [arXiv:1905.02078] [INSPIRE].

[34] A. Lewis, A. Challinor and A. Lasenby, *Efficient computation of CMB anisotropies in closed FRW models*, *Astrophys. J.* **538** (2000) 473 [astro-ph/9911177] [INSPIRE].

[35] J. Koda et al., *Are peculiar velocity surveys competitive as a cosmological probe?*, *Mon. Not. Roy. Astron. Soc.* **445** (2014) 4267 [arXiv:1312.1022] [INSPIRE].

[36] J. Bel et al., *Accurate fitting functions for peculiar velocity spectra in standard and massive-neutrino cosmologies*, *Astron. Astrophys.* **622** (2019) A109 [arXiv:1809.09338] [INSPIRE].

JCAP09(2025)005

[37] Planck collaboration, *Planck 2018 results. VI. Cosmological parameters*, *Astron. Astrophys.* **641** (2020) A6 [*Erratum ibid.* **652** (2021) C4] [arXiv:1807.06209] [INSPIRE].

[38] Y. Lai, C. Howlett and T.M. Davis, *Using peculiar velocity surveys to constrain the growth rate of structure with the wide-angle effect*, *Mon. Not. Roy. Astron. Soc.* **518** (2022) 1840 [arXiv:2209.04166] [INSPIRE].

[39] LSST Dark Energy Science collaboration, *Type Ia supernova growth-rate measurement with LSST simulations: intrinsic scatter systematics*, arXiv:2505.13290 [INSPIRE].

[40] L. Dam, K. Bolejko and G.F. Lewis, *Exploring the redshift-space peculiar velocity field and its power spectrum*, *JCAP* **09** (2021) 018 [arXiv:2105.12933] [INSPIRE].

[41] C. Pryor and G. Meylan, *Velocity Dispersions for Galactic Globular Clusters*, in *Astronomical Society of the Pacific Conference Series. Vol. 50: Structure and Dynamics of Globular Clusters*, S.G. Djorgovski and G. Meylan eds., Astronomical Society of the Pacific (1993), pg. 357.

[42] P.J. Godwin and D. Lynden-Bell, *Evidence of a small velocity dispersion for the Carina dwarf spheroidal?*, *Mon. Not. Roy. Astron. Soc.* **229** (1987) 7.

[43] A. Spurio Mancini et al., *CosmoPower: emulating cosmological power spectra for accelerated Bayesian inference from next-generation surveys*, *Mon. Not. Roy. Astron. Soc.* **511** (2022) 1771 [arXiv:2106.03846] [INSPIRE].

[44] J.D. Talman, *Numerical Fourier and Bessel transforms in logarithmic variables*, *J. Comput. Phys.* **29** (1978) 35.

[45] X. Fang, E. Krause, T. Eifler and N. MacCrann, *Beyond Limber: Efficient computation of angular power spectra for galaxy clustering and weak lensing*, *JCAP* **05** (2020) 010 [arXiv:1911.11947] [INSPIRE].

[46] J. Bradbury, et al., *JAX: composable transformations of Python+NumPy programs*, (2018).

[47] R. Frostig, M. Johnson and C. Leary, *Compiling machine learning programs via high-level tracing*, *SysML* (2018).

[48] D. Foreman-Mackey, D.W. Hogg, D. Lang and J. Goodman, *emcee: The MCMC Hammer*, *Publ. Astron. Soc. Pac.* **125** (2013) 306 [arXiv:1202.3665] [INSPIRE].

[49] J. Goodman and J. Weare, *Ensemble samplers with affine invariance*, *Commun. Appl. Math. Comput. Sc.* **5** (2010) 65 [INSPIRE].

[50] D. Piras and A. Spurio Mancini, *CosmoPower-JAX: high-dimensional Bayesian inference with differentiable cosmological emulators*, arXiv:2305.06347 [DOI:10.21105/astro.2305.06347] [INSPIRE].

[51] G.L. Jones and Q. Qin, *Markov Chain Monte Carlo in Practice*, *Ann. Rev. Statist. Appl.* **9** (2022) 557.

[52] S.R. Hinton, *ChainConsumer*, *J. Open Source Softw.* **1** (2016) 45.

[53] Planck collaboration, *Planck intermediate results. XVI. Profile likelihoods for cosmological parameters*, *Astron. Astrophys.* **566** (2014) A54 [arXiv:1311.1657] [INSPIRE].

[54] M.C. March et al., *Improved constraints on cosmological parameters from SNIa data*, *Mon. Not. Roy. Astron. Soc.* **418** (2011) 2308 [arXiv:1102.3237] [INSPIRE].

[55] J. Adamek, D. Daverio, R. Durrer and M. Kunz, *gevolution: a cosmological N-body code based on General Relativity*, *JCAP* **07** (2016) 053 [arXiv:1604.06065] [INSPIRE].

JCAP09(2025)005

[56] J. Adamek et al., *Bias and scatter in the Hubble diagram from cosmological large-scale structure*, *Phys. Rev. D* **100** (2019) 021301 [arXiv:1812.04336] [INSPIRE].

[57] J. Jonsson et al., *Constraining dark matter halo properties using lensed SNLS supernovae*, *Mon. Not. Roy. Astron. Soc.* **405** (2010) 535 [arXiv:1002.1374] [INSPIRE].

[58] F. Sorrenti, R. Durrer and M. Kunz, *The dipole of the Pantheon+SH0ES data*, *JCAP* **11** (2023) 054 [arXiv:2212.10328] [INSPIRE].

[59] F. Sorrenti, R. Durrer and M. Kunz, *A local infall from a cosmographic analysis of Pantheon+*, *JCAP* **12** (2024) 003 [arXiv:2407.07002] [INSPIRE].

[60] L. Verde, T. Treu and A.G. Riess, *Tensions between the Early and the Late Universe*, *Nature Astron.* **3** (2019) 891 [arXiv:1907.10625] [INSPIRE].

[61] W.L. Freedman et al., *Status Report on the Chicago-Carnegie Hubble Program (CCHP): Measurement of the Hubble Constant Using the Hubble and James Webb Space Telescopes*, *Astrophys. J.* **985** (2025) 203 [arXiv:2408.06153] [INSPIRE].

[62] A.G. Riess et al., *JWST Validates HST Distance Measurements: Selection of Supernova Subsample Explains Differences in JWST Estimates of Local H_0*, *Astrophys. J.* **977** (2024) 120 [arXiv:2408.11770] [INSPIRE].

[63] W. Freedman, *The expanding Universe — do ongoing tensions leave room for new physics?*, *Nature* **639** (2025) 858 [INSPIRE].

[64] LSST Science and LSST Project collaborations, *LSST Science Book, Version 2.0*, arXiv:0912.0201 [INSPIRE].

[65] G. Jelic-Cizmek, F. Lepori, J. Adamek and R. Durrer, *The generation of vorticity in cosmological N-body simulations*, *JCAP* **09** (2018) 006 [arXiv:1806.05146] [INSPIRE].

[66] R. Tripp, *A Two-parameter luminosity correction for type Ia supernovae*, *Astron. Astrophys.* **331** (1998) 815 [INSPIRE].

[67] R.B. Tully and J.R. Fisher, *A New method of determining distances to galaxies*, *Astron. Astrophys.* **54** (1977) 661 [INSPIRE].

[68] S. Djorgovski and M. Davis, *Fundamental properties of elliptical galaxies*, *Astrophys. J.* **313** (1987) 59 [INSPIRE].

[69] A. Dressler et al., *Spectroscopy and photometry of elliptical galaxies. 1. A New distance estimator*, *Astrophys. J.* **313** (1987) 42 [INSPIRE].

[70] R.B. Tully et al., *Cosmicflows-4*, *Astrophys. J.* **944** (2023) 94 [arXiv:2209.11238] [INSPIRE].

JCAP09(2025)005